Monitoring and Modeling of Creaming in Oil-in-Water Emulsions

Tanmoy Kanti Deb, Noureddine Lebaz, Mahir Sinan Ozdemir, Ruxandra Govoreanu, Adel Mhamdi, Gürkan Sin, Nida Sheibat-Othman

Monitoring and modeling of creaming in oil-in-water emulsions

Tanmoy Kanti Deb[1], Noureddine Lebaz[1], Mahir Sinan Ozdemir[2], Ruxandra Govoreanu[2], Adel Mhamdi[3], Gürkan Sin[4], Nida Sheibat-Othman[1*]

[1]University of Lyon, Université Claude Bernard Lyon 1, CNRS, LAGEPP UMR 5007, 69100 Villeurbanne, France
[2]Pharmaceutical Development & Manufacturing Sciences, Janssen Research & Development, 2340 Beerse, Belgium
[3] AVT.SVT, RWTH Aachen University, 52062 Aachen, Germany
[4]Departement of Chemical and Biochemical Engineering, Technical University of Denmark, Kongens Lyngby 2800, Denmark
[*]Correspondence : Dr Nida Sheibat-Othman (e-mail : nida.othman@univ-lyon1.fr)

Abstract

This work combines experimental and modeling investigations to monitor the dynamics of creaming in oil-in-water emulsions. Turbidity and Raman spectroscopy methods were compared for the experimental monitoring of creaming of n-hexadecane droplets in water. A creaming model is developed based on the convection-diffusion equation. The model accounts for the full droplet size distribution. The experimental data were used to identify the diffusion coefficient of the oil droplets and the Richardson-Zaki coefficient correcting the effect of the local volume fraction. The droplets size and concentration are varied to evaluate their effect on the creaming rate. The developed model could accurately predict the kinetics of creaming in the different considered cases. It can be used for emulsion stability studies for instance in food / pharmaceutical industries and/or for gravity separators design and monitoring.

1 Introduction

Emulsions are immiscible liquid-liquid dispersions used in a widespread range of applications such as food, cosmetics and pharmaceutics. They are also used as intermediate steps in various industries like liquid-liquid extraction or as a mean to enhance oil recovery in crude oil production [1]. They are heterogeneous systems where liquid droplets (constituting the dispersed phase) are dispersed in a liquid medium (the continuous phase) and stabilized by surface active

agents. Emulsions are usually thermodynamically unstable and tend continuously toward lower energy states, which may ultimately lead to phase separation [2]. After their formulation, the dispersed droplets may experience different mechanisms including coalescence, flocculation, growth by Ostwald ripening affecting the droplet size distribution (DSD), which represents one of the important emulsion properties. They may also undergo creaming or sedimentation, which affects the spatial uniformity of the emulsion[3].

The stability against droplet coalescence can be improved by using emulsifying agents that reduce the interfacial tension between the two immiscible liquids. Such emulsifiers usually do not ensure stability against creaming / sedimentation, where the driving force is the difference in density between the two phases, which causes the movement of the droplets under gravity, and leads to non-uniform spatial distribution of the emulsion [4]. For instance, in oil-in-water (O/W) emulsions, oil is usually less dense than water so oil droplets move upwards and accumulate at the top of the emulsion; this phenomenon is referred to as creaming [5]. Once droplets are accumulated in the top or in the bottom of the container, the probability of their coalescence increases.

Monitoring and modeling of creaming is of high practical importance [6,7], and represents the focus of this work. Indeed, in many applications a stable uniform emulsion is required, and there are applications where separation of phases is desired (by creaming / sedimentation, coagulation). In both cases, it is important to monitor and model these phenomena and to predict their occurrence (i.e. changes in the spatial distribution of the droplets or their size). For instance, in food or pharmaceutical applications, the uniformity of the emulsion may affect the product properties (taste, bioavailability, etc.). On the other hand, in processes where it is required to separate the oil and the water phases, it is important to evaluate the impact of the operating conditions on the separation rate [8,9].

The challenges in modeling creaming processes lie in their complexity (e.g. polydispersity of the droplets size, the difficulty to quantify droplet-droplet and droplet-continuous phase interactions) and the lack of non-invasive and quantitative measurement techniques [5,10]. To characterize the stability of emulsions, different analytical techniques and methodologies were evaluated mainly offline [5], including turbidimetry [3,11,12], nuclear magnetic resonance (NMR) [13–15], optical imaging [16,17], electric conductivity [18] and ultrasonic measurements [19,20]. Vibrational spectroscopy, such as infrared or Raman spectroscopy, was also investigated to characterize emulsion-based products, but mainly for the determination of their components[21]. The turbidimetry is the mainly used technology for its high precision and wide range of applicability. However, it is sensitive to both the droplet size and concentration, and may not operate well in concentrated media. Electric conductivity is very interesting, but its use is limited to charged emulsions. The ultrasonic technique is precise, but sensitive to impurities and variation in temperature, and the existing technologies are limited to dilute emulsions and big droplet size. Regarding optical imaging, it is mainly qualitative since image processing is time consuming, and it is limited to dilute emulsions (less than ~10 %) and cannot detect droplets smaller than ~ 10 µm. However, it gives information also about the shape of the droplets. Spectroscopy appears to represent a good alternative for online and *in situ* monitoring of the creaming process and will therefore be considered in this work. It will be compared to offline turbidimetry.

Models with different complexity levels are available to describe the creaming process [22,23]. The creaming velocity of an isolated rigid spherical particle in an ideal stagnant fluid can be determined by Stokes law[24]. Then, modifications were proposed to account for the effect of the dispersed phase concentration [25,26]. Kynch proposed a mathematical approach to deal with the local particle concentration in batch sedimentation [27]. Later, colloidal particles of polydisperse sizes following a Gaussian distribution were considered [28]. Indeed, it is required to consider the

full size distribution of the droplets, as the velocity of droplets of similar chemical composition is mainly governed by their size [29]. This model was then extended for multiple population droplets [16]. Modeling of creaming / sedimentation in liquid-liquid systems finds an interest also in gravity separators [30,31]. Models including creaming / sedimentation combined with binary and interfacial coalescence phenomena were also employed [32,33]. If the creaming / sedimentation process involves changes in the particle / droplet size (ex. coagulation), the use of the population balance modeling (PBM) framework becomes attractive to describe these coupled phenomena while accounting for the polydisperse nature of the droplets size [33–35]. For instance, Grimes et al. employed the full distribution to describe batch gravity separation of crude oil-in-water emulsions and concluded that the degree of polydispersity is a key factor in determining the rate of coalescence and separation by sedimentation [35]. Finally, coupling of PBMs with computational fluid dynamics (CFD) constitutes an accurate way to describe the coupled phenomena of diffusion in space and changes in the droplet size, but this approach still remains computationally intensive [20,36].

From the literature analysis, it appears that there is a need to develop *in situ* sensors to monitor the creaming phenomenon and predict the model parameters under a wide range of operating conditions. In this study, emulsions of hexadecane in water are considered as a model system at different oil fractions and droplet sizes. The convection-diffusion equation is used to describe creaming of oil droplets, assuming that no change in the droplet size occurs during creaming. Indeed, coalescence could be prevented over the studied period by using an adapted surfactant, and Ostwald ripening was found to be negligible due to the low solubility of the used oil in water at the considered temperature. This was validated by measuring the droplets size distribution after the creaming study, where it was found that no change occurred during creaming. Thus, the evolution of the DSD at any position in the cell could be related to creaming only. Experimental monitoring is ensured by turbidimetry and Raman spectroscopy. The

diffusion and the Richardson-Zaki coefficients are identified for the different operating conditions.

2 Materials and experimental methods

2.1 Materials

n-Hexadecane (Table 1) was used as dispersed phase, and polyethylene glycol sorbitan monolaurate (Tween® 20) as surfactant (both purchased from Sigma-Aldrich, Germany). Deionized (DI) water (Millipore Direct-Q3 Deionized Water Unit) was used for all preparations as continuous phase, with conductivity ≈ 5.47 μS.m^{-1} at 25 °C.

2.2 Preparation of emulsions

Oil-in-water emulsions were prepared at room temperature by dispersing n-hexadecane in deionized water in which the surfactant is previously dissolved. The amount of surfactant is calculated to ensure saturation of water as well as a monolayer coverage of the surface of droplets with 10 % excess. The surface area of droplets per unit volume of emulsion is: $A_{\mathrm{d}}(\mathrm{m}^2/\mathrm{m}^3) = 6\phi/d_{43}$. So, the amount of surfactant required to ensure the full coverage of the droplets' surface is: $m_{\mathrm{s}}(\mathrm{kg}/\mathrm{m}^3) = A_{\mathrm{d}} M_{\mathrm{w,s}}/(a_{\mathrm{s}} N_{\mathrm{a}})$, where N_{a} is the Avogadro number, a_{s} the surface coverage of one molecule of surfactant (1.33×10^{-18} m²) and $M_{\mathrm{w,s}}$ its molecular weight. To this amount, the critical micellar concentration of surfactant (0.058 mM at 20 °C [37]) is added to saturate the water phase, as well as 10 % excess. As a result, to form an emulsion with $\phi = 0.1$ and $d_{43} = 1$ μm, the minimal required concentration of surfactant is 1.1 g L^{-1}. Therefore, it was decided to use 2 g L^{-1} for emulsions with the different sizes. The emulsions with other fractions are obtained by dilution of these concentrated emulsions. The interfacial tension of the emulsions was about 4.8 mN m^{-1} and the viscosity of the continuous phase (water and surfactant) is ~ 1 mPa.s.

First, a pre-mix was prepared by mixing oil in the continuous phase using a magnetic stirrer. Then, further homogenization was obtained using a high-speed mixer (Ultra-Turrax T25 basic, IKA Corp.) equipped with a rotor-stator type dispersion tool (18G, IKA Corp.). The homogenization speed and the total homogenization time ranged from 3 000-22 000 rpm and 3 to 25 minutes respectively to generate different droplet sizes. The resulting emulsions had mean sizes of $d_{43} = 1$, 3.6, and 6.9 µm, with standard deviation $\sigma \approx 1.2$, 2.4, and 6 µm, respectively (where d_{43} is the volume-weighted mean particle size, also called the De Brouckere mean diameter). These emulsions (10 % in volume) were diluted at about 1, 3, and 6 % in volume.

Table 1: Properties of n-hexadecane ($C_{16}H_{34}$)

Molecular weight (kg mol^{-1})	0.226
Density (kg m^{-3})	773
Dynamic viscosity (mPa.s) at 20°C	3.032
Melting temperature (°C)	18

2.3 Droplet size distribution (DSD) measurement

The DSD of the emulsions were measured by laser diffraction (Mastersizer 3000, Malvern Corp.). After preparation, the emulsions were kept at rest for few minutes prior to the measurement, and shook by hand when taking a sample. A similar measurement was made after creaming to confirm no change in the droplet size with time.

2.4 Monitoring of creaming

The creaming was monitored using two methods: Turbidimetry and Raman spectroscopy, using the same bottles and at the same temperature. Indeed, turbidimetry can precisely evaluate the concentration of oil and may allow to identify the model parameters[3,11,12]. Also, it is aimed to

evaluate the potential of Raman spectroscopy for *in situ* monitoring of creaming, while turbidimetry will be used offline.

The used Turbiscan Lab Expert (Formulaction®, France) is based on multiple light scattering analysis, with an incident light constituted of a pulse of near infrared monochromatic light source of wavelength 850 nm[38]. It was used to collect the transmitted (T) and backscattered (BS) fractions of the incident light, using detectors mounted respectively at angles 0° and 135° with respect to the incident beam. The device scans the entire height of the cell containing the emulsion (of height 54 mm) with a 40 µm interval. A full scan is done every minute. Experiments were carried out at a constant temperature of 20 °C. A scheme showing an example of backscattering is shown in Figure 1.

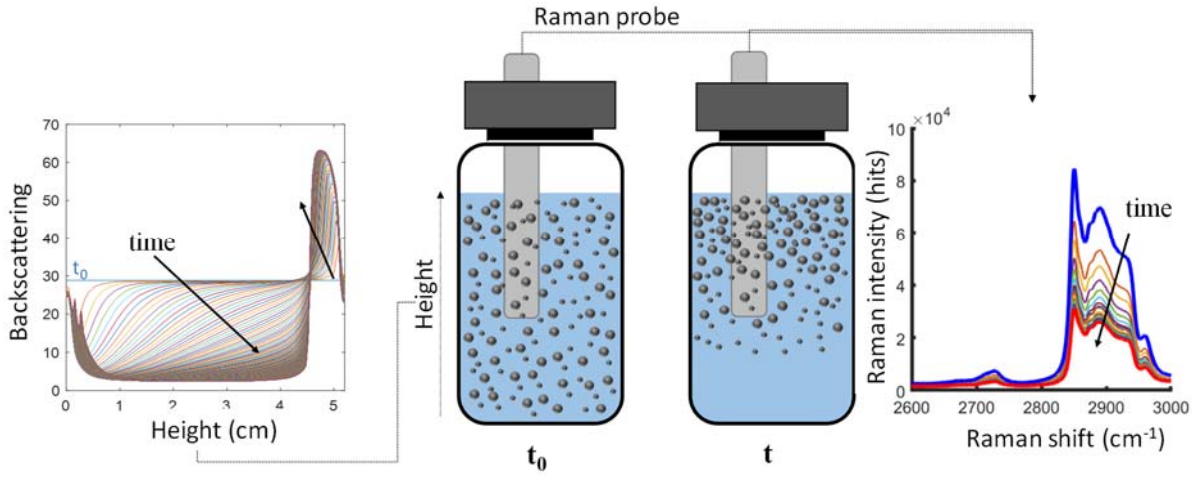

Figure 1: A schematic representation of a creaming emulsion, with an example of backscattering measured with time and over height, and an example of Raman spectra measured with time at a fixed height.

A Raman spectrometer, RXN2 Raman Analyzer, Kaiser Optical Systems (Ann Arbor, USA) was used. It is equipped with a charge-coupled device camera and a diode laser, and operates at a wavelength of 785 nm with a laser power of 400 mW. The software HoloPro 3.2 is used

for data collection. A scan is done every 200 seconds. Acquisition was achieved by two probing modes:

- The first mode, called wet head mode (WH), consists of direct immersion of the Raman probe in the emulsion, at height 2.5 cm from the bottom of the sample, and the sample was put in a well-designed chamber to exclude any ambient light, and measured at room temperature.
- The second mode is called non-contact optical (NC) mode, where the sample was put into a cell located inside the spectrometer, kept at 20 °C. A distance of 0.2 cm between the diamond tip and the surface of the emulsion container was maintained in non-contact measurements, and scanned at about the middle of the bottle.

3 Model of the creaming process

In Kynch's theory[27], the settling velocity is determined by the local dispersed phase concentration, with the assumptions of droplets of same size, shape and density, the suspension being incompressible and the flow one-dimensional. Following Kynch's theory, the one-dimensional sedimentation process can hence be described by the following continuity equation:

$$\frac{\partial \phi}{\partial t} + \frac{\partial (u\,\phi)}{\partial z} = 0 \qquad (1)$$

where $\phi(z,t)$ is the dispersed phase volume fraction at a given time t and position z (the spatial axis in the vertical direction), and $u(\phi,d)$ is the hindered velocity of the dispersed droplets which also depends on the droplet diameter d. In addition to the dispersed phase convective flux, Davis et al.[28] considered the effect of diffusion of the particles due to Brownian motion which acts against creaming or sedimentation:

$$\frac{\partial \phi}{\partial t} + \frac{\partial (u\,\phi)}{\partial z} = \frac{\partial}{\partial z}\left(D\,\frac{\partial \phi}{\partial z}\right) \qquad (2)$$

where D is the diffusion coefficient.

To take into account the polydispersity in the droplets size, equation 2 becomes:

$$\frac{\partial \phi_i}{\partial t} + \frac{\partial (u_i\, \phi_i)}{\partial z} = \frac{\partial}{\partial z}\left(D_i \frac{\partial \phi_i}{\partial z}\right) \quad (3)$$

where the index i refers to the properties of droplets having a diameter d_i.

The creaming velocity, u_i, can be hindered by the dispersed phase volume fraction as follows[26,39]:

$$u_i(z,t) = u_{ti}\left(1 - \frac{\phi_T}{\phi_{max}}\right)^n \quad (4)$$

where n is the Richardson-Zaki constant[26] and $\phi_T(z,t) = \sum \phi_i(z,t)$ is the fraction of all oil droplets at time t and position z . ϕ_{max} is the maximal possible volume fraction, which is introduced because the local total fraction $\phi_T(z,t)$ does not reach unity during the considered creaming time, whatever the DSD or the position in the container, as droplet coalescence is prevented. u_{ti} is the terminal velocity of a droplet of diameter d_i moving in an ideal stagnant infinite fluid (i.e. when the buoyancy, drag and gravity forces are in equilibrium), given by Stokes law:

$$u_{ti}(z,t) = -\frac{(\rho_d - \rho_c) d_i^2 g}{18\mu} \quad (5)$$

where ρ_d and ρ_c are the densities of the dispersed and continuous phases respectively, g is the gravity acceleration and μ is the apparent viscosity of the emulsion given by[40]:

$$\mu(z,t) = \mu_c\left[1 + 2.5\, \phi_T(z,t)\left(\frac{\mu_d + 2/5\mu_c}{\mu_d + \mu_c}\right)\right] \quad (6)$$

Note that when the local volume fraction of the dispersed phase tends to zero, the creaming velocity u_i becomes equal to the terminal velocity u_{ti}. Inversely, if the local volume fraction tends to its maximum value, the droplets are trapped among each other and stop moving (i.e. $u_i = 0$). In this study, the oil dispersed phase is less dense than the continuous phase

constituted of water, thus the difference $(\rho_{\mathrm{d}} - \rho_{\mathrm{c}})$ is negative which means that the oil droplets are rising through the continuous phase.

Note that the diffusion term has a lower effect on creaming compared to the convection term. Therefore, one may assume that the diffusion of one droplet is not hindered by the presence of other droplets, so there is no need to make a correction for the volume fraction as done for the velocity. Moreover, droplets in an emulsion with a narrow size distribution can be assumed to have one constant diffusion coefficient D, instead of a specific coefficient D_i for each droplet size. Therefore, simulations with a finer modeling of the diffusion coefficient did not impact measurably the results, but increased the computation time only.

By substituting equation 4 into 3, one gets the following equation, used in this work:

$$\frac{\partial \phi_i}{\partial t} + \frac{\partial\left(u_{\mathrm{t}i}\phi_i\left(1-\frac{\phi_{\mathrm{T}}}{\phi_{\max}}\right)^n\right)}{\partial z} = \frac{\partial}{\partial z}\left(D\frac{\partial \phi_i}{\partial z}\right) \qquad (7)$$

The initial condition of equation 7 assumes spatial uniformity, i.e. the droplets of different sizes are equally distributed in the entire spatial domain. The boundary condition of the net flux of droplets at the top and at the bottom of the cells is zero. The model equations were solved using the Matlab® function *pdepe*. The simulated cell dimension is 5.4 cm of height, for a duration of 4 hours, and the height of the cell is divided into intervals of 0.004 cm. The discretization used for the droplet size distribution is the logarithmic one obtained experimentally by the Mastersizer (giving 30-35 classes depending on the droplet size distribution).

The unknown parameters in equation 7 are the diffusion coefficient D and the Richardson-Zaki constant n, that need to be identified based on experimental measurements of creaming with time (i.e. using $\phi_{\mathrm{T}}(z,t)$). For parameter identification, the non-linear optimization solver *lsqnonlin* of the Matlab® Global Optimization Toolbox was used.

4 Results and discussion

Emulsions were prepared with different mean sizes: $d_{43} = 1$, 3.6 and 6.8 µm, and were diluted to get volume fractions of about: $\phi = 1$, 3, 6, and 10 % vol., thus giving 12 samples. Two identical bottles were filled with each sample (up to height 5.4 cm), one is used for monitoring by Turbiscan (at 20°C) and the other by Raman spectroscopy. The wet head Raman probe was inserted at 2.5 cm (at ambient temperature) while for the non-contact Raman, the bottle was put into the device where scanning occurs approximately at the same height (at 20°C). The samples were monitored for 4 hours. The droplets size was measured after the creaming study to validate that no coalescence occurred during creaming. As the melting temperature of n-hexadecane is 18 °C, it is in the liquid state during the study.

4.1 Monitoring of creaming by Raman spectroscopy

Hexadecane, in its liquid state, is known to give peaks in the Raman spectrum in the CH stretching region (2848, 2873, 2886, 2930, 2957 cm^{-1}) and in the fingerprint vibrational region (1060, 1074, 1128, 1296, 1435 cm^{-1})[41]. The evolution of the Raman spectra in both regions using the *in situ* probe, in the case of emulsion of mean diameter 6.8 µm, is shown in Figure 2 for the volume fraction of $\phi = 2.56$ %, and Figure 3 for $\phi = 7.4$ %. It can be seen that the higher is the concentration of oil, the bigger becomes the surface area of the peaks in both regions. The creaming leads to the reduction of the amount of oil at the measurement location (2.5 cm height), so the amplitudes of the peaks decrease with time. It appears therefore that *in situ* Raman spectroscopy is appropriate to monitor creaming in this system.

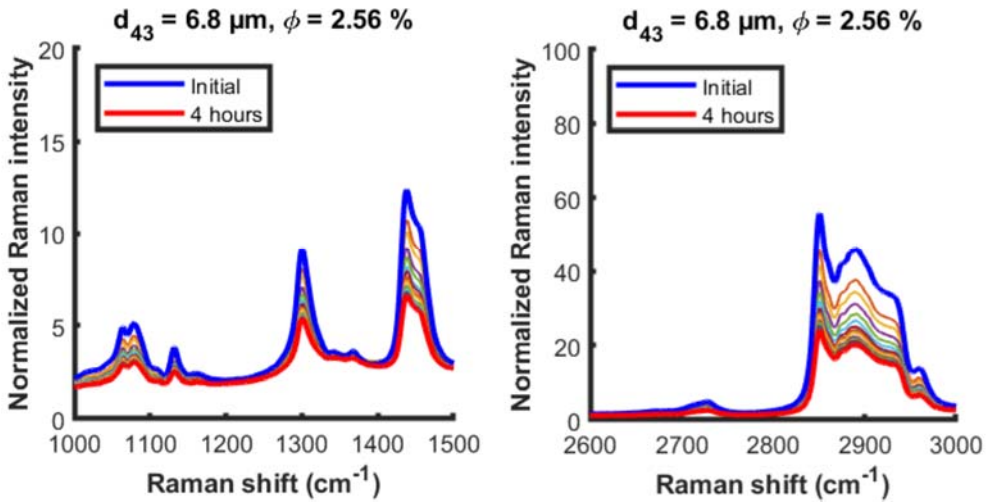

Figure 2: Evolution of the Raman spectra during creaming using the wet head in situ probe, placed at height 2.5 cm from the bottom of the cell, sample with $d_{43} = 6.8$ *µm and* $\phi =$ 2.56 %.

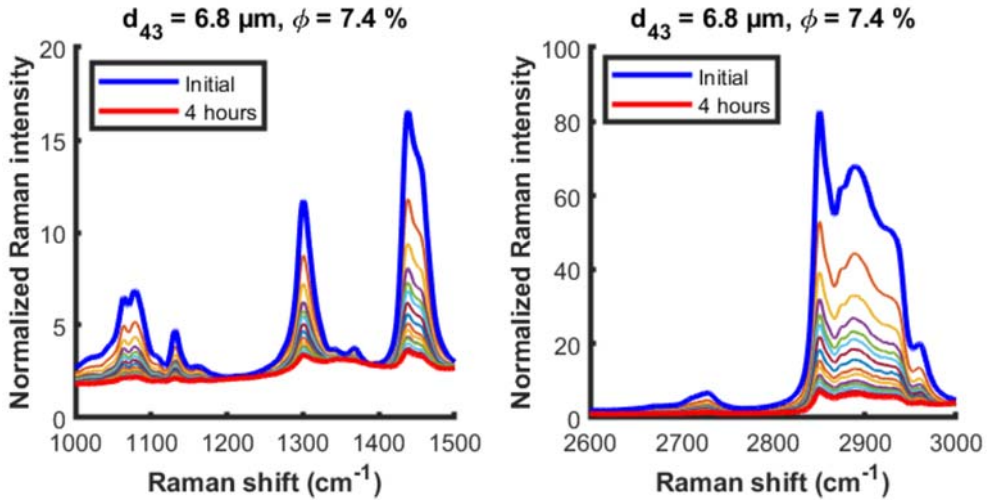

Figure 3: Evolution of the Raman spectra during creaming using the wet head in situ probe, placed at height 2.5 cm from the bottom of the cell, sample with $d_{43} = 6.8$ *µm and* $\phi =$ 7.4 %.

Figure 4 shows the results obtained by the non-contact Raman spectrometer in the CH stretching region where the initial and final spectra are compared for samples with different droplet sizes and fractions. Regarding the fingerprint vibrational region, it was found to be affected by the glass wall of the bottle and difficult to exploit in non-contact mode. First, it can be seen that the sample of $d_{43} = 1$ µm is stable over time at a fraction of 6 % vol., and this was the case for all fractions considered in this work (1 to 10 % vol.) with this mean droplet size. The samples with other sizes are not stable against creaming, as the signal of oil decreases importantly with time

at the measurement height. The amplitude of the oil signal increases when increasing its concentration in this device as well. But, the amplitude is much lower than in the *in situ* probe, and is therefore less sensitive to changes. However, the non-contact probe has the advantage of being non-invasive, therefore, it does not affect the hydrodynamics of creaming and the oil droplets may not coalesce on the probe itself or obstruct it, which may occur in the *in situ* probe.

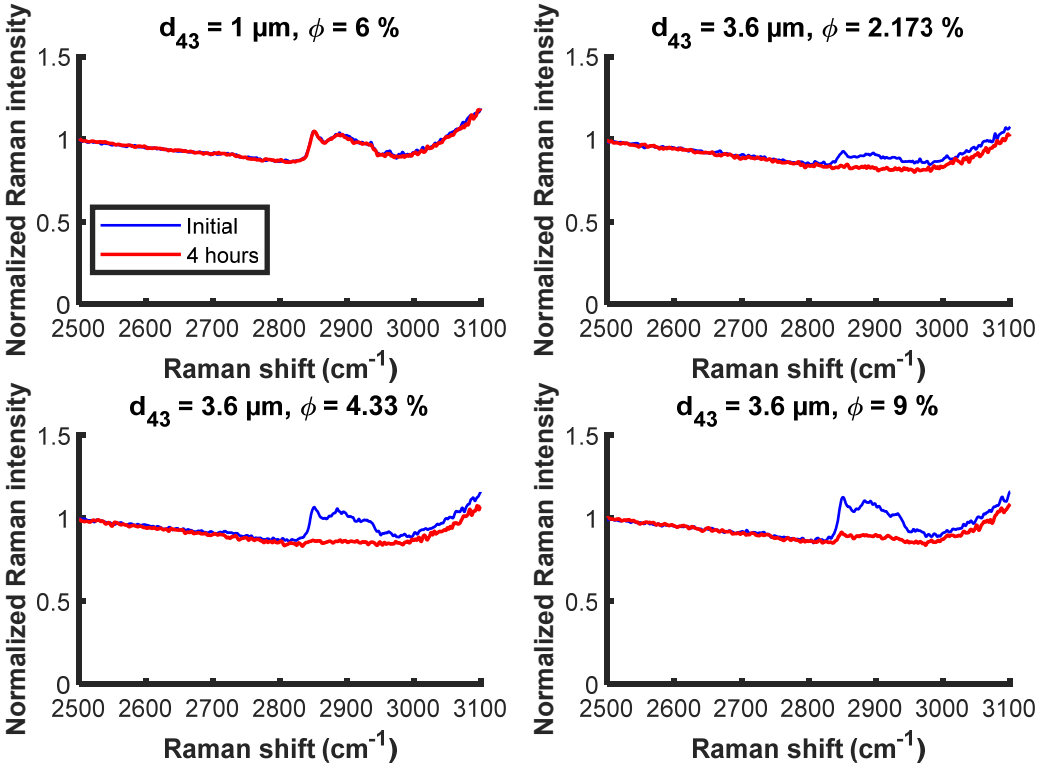

Figure 4: Initial and final Raman spectra during creaming (non-contact probe, at approximately mid-height from the bottom of the bottle).

Based on Raman analysis, it could be seen that the sample of 1 µm of mean droplet diameter was stable at all studied concentrations, as the spectra did not evolve during the measurement period, while in the samples of 3.6 µm and 6.8 µm creaming occurred with all concentrations. In general, noisier data were observed for bigger droplets, but the effect of size on the spectra was relatively small. Therefore, the surface area of the peak between 2 800 and 3 000 cm^{-1} was found to increase almost linearly with the concentration of oil. Therefore, the following simple

relationship can be employed to predict the oil fraction from the Raman spectra (measured only at $z = 2.5$ cm):

$$\phi_{\mathrm{T}}(z,t) = \frac{\phi_{\mathrm{T}}(t_0)S(t)}{S(t_0)} \quad (1)$$

Where $\phi_{\mathrm{T}}(t_0)$ is the initial volume fraction that is assumed to be known as the sample is initially uniform. $S(t_0)$ and $S(t)$ represent the surface area of the pic of between 2 800 and 3 000 cm^{-1} at time t_0 and at time t, respectively. A comparison of Raman predictions with Turbiscan and the model is shown in the last section.

4.2 Monitoring of creaming by turbidimetry

The Turbican measurements confirmed that the samples with mean diameter of 1 μm were stable against creaming over 4 hours (as the backscattering signal was constant over time and height), so they will not be discussed here. In this section, the focus will be on the samples with the mean sizes $d_{43} = 3.6$ and 6.8 μm, for which two different calibrations were realized to predict the volume fraction $\phi_{\mathrm{T}}(z,t)$ from the backscattering data. To do so, different concentrations were prepared (by simple dilution of an initially concentrated emulsion) for each droplet size and analyzed by turbidimetry. A polynomial of order four was extracted to relate the backscattering signal to the volume fraction. By this way, recorded backscattering data were transformed to volume fractions at each height and with time. Note that the turbidimetry measurement is very sensitive to the droplet size, so different calibrations are done for the emulsions with different mean diameters.

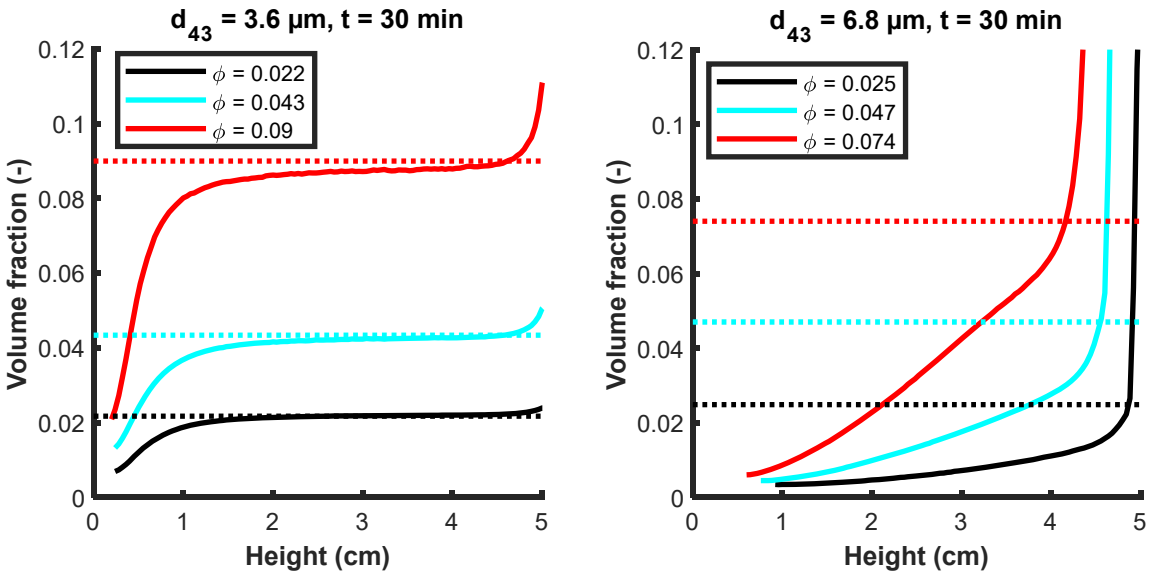

Figure 5: Evolution of the volume fraction of oil at different heights in the bottle, for different sizes and initial concentrations as monitored by Turbiscan after calibration: dotted line is the initial fraction and the continuous line is after 30 min of storage.

The effects of the droplet size and dispersed phase volume fraction on the dynamics of creaming are shown in Figure 5. It can be seen that the volume fraction gradually decreases at the bottom of the sample and increases at the top, at different speeds for the different samples. The extent of creaming is much higher for bigger droplets, while smaller droplets are more stable. Also, more diluted emulsions seem to cream faster, see for instance droplets of 6.8 µm, where with a volume fraction of 7.4 %, the emulsion is more stable than with 2.5 % that completely cleared at the bottom after 30 minutes. The measurement at the bottom of the sample was cut as it was affected by the glass base of the container (0.3 cm). Also, when the backscattering signal becomes very low, it is not to be used, and it is advised to rely on the transmission signal in this case. This occurs for instance when full creaming happens, which means that the concentration of droplets is at its minimal value. When this occurs, the signal is cut and not interpreted in this region.

4.2 Modeling and simulation results

To solve equation 7, we need to determine the maximal fraction of droplets in the creaming layer, $\phi_{\max}$, the diffusion coefficient D and the Richardson-Zaki constant n. Random packing of monodisperse spheres is known to vary between 0.52 and 0.64, and to reach 0.74 for the densest regular packing. In the case of emulsions stabilized by surfactants, the surfactant layer allows to keep the droplets far from each other, which may reduce the packing density. Note that complex phenomena may occur in the packed region, such as droplet deformation and coalescence which may increase the fraction of oil in this region, to reach ultimately $\phi_{\max} = 1$. As it was checked that no coalescence occurs during the creaming study, the maximal fraction may not reach 1 in our case. Simulations of the creaming model were performed using different values of $\phi_{\max}$ (0.35, 0.45, 0.55 and 1), (Figure 6), and it can be seen that there is little difference between the creaming profiles obtained with $\phi_{\max} = 0.45$ and 0.55, so the value of $\phi_{\max} = 0.45$ will be used in the model. Indeed, this parameter would be difficult to identify precisely from the experimental data as it has little impact on the creaming profile in the present study.

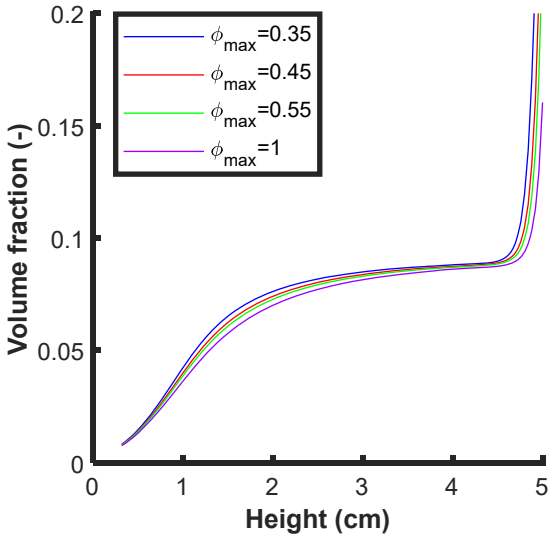

Figure 6: Effect of ϕ_{max} on the creaming profile. Simulation of an experiment with 9 % oil, $d_{43} = 3.6$ µm, after one hour of creaming.

The other unknown parameters, the diffusion coefficient *D* and the Richardson-Zaki constant n, will be identified based on experimental data of the turbidimetry. Parameter identification was done for the two experiments with the highest fractions, as this gives the best identifiability of the parameter n (one experiment with $\phi = 9$ % and $d_{43} = 3.6$ µm, and one with $\phi = 7.4$ % and $d_{43} = 6.8$ µm). The identification results are shown in Table 2. It can be seen that a slightly higher value of the Richardson-Zaki constant, n, is identified for bigger droplets. This parameter indicates the impact of the volume fraction on the velocity through the term $[1 - \phi_{\mathrm{T}}/\phi_{\mathrm{max}}]^n$. The volume fraction seems to impact the creaming to a greater extent when the droplets are bigger, which is plausible as the motion of bigger droplets can more easily be hindered by the presence of obstacles (i.e. other droplets). Richardson and Zaki identified $n = 4.65$[26], while Aleem and Mellon indicated that it may vary between 2.3-5.5, and identified $n = 5.1$ in their experiments[4]. Here, a lower value of n is obtained, probably due to a different range of droplet diameters.

A higher diffusion coefficient is identified for bigger droplets (Table 2). Following Stokes-Einstein law, the diffusion coefficient should be higher for smaller particles. However, decreasing the droplet size may increase the apparent viscosity of the suspension[42], that is not accounted for in equation 6.

Table 2: Identified model parameters for experiments with mean droplet size $d_{43} = 3.6$ and 6.8 µm (values are valid for the different volume fractions, $\phi = 3, 6, 10$ %).

d_{43} (µm)	D (m² s^{-1})	n
3.6	1×10^{-9}	1

6.8	8×10^{-9}	1.5

Figure 7 shows the model validation results using the parameters identified in Table 2, for six experiments with different initial oil concentrations and mean droplet sizes. It can be seen that samples with smaller droplets are more stable, as the volume fraction remains more uniform over height for a longer duration. Also, increasing the concentration of droplets enhances the stability of the sample against creaming. An acceptable prediction is obtained under the different conditions, which indicates that the model is adapted in this range of operation. A better fit is obtained for smaller particles, independently of the oil fraction.

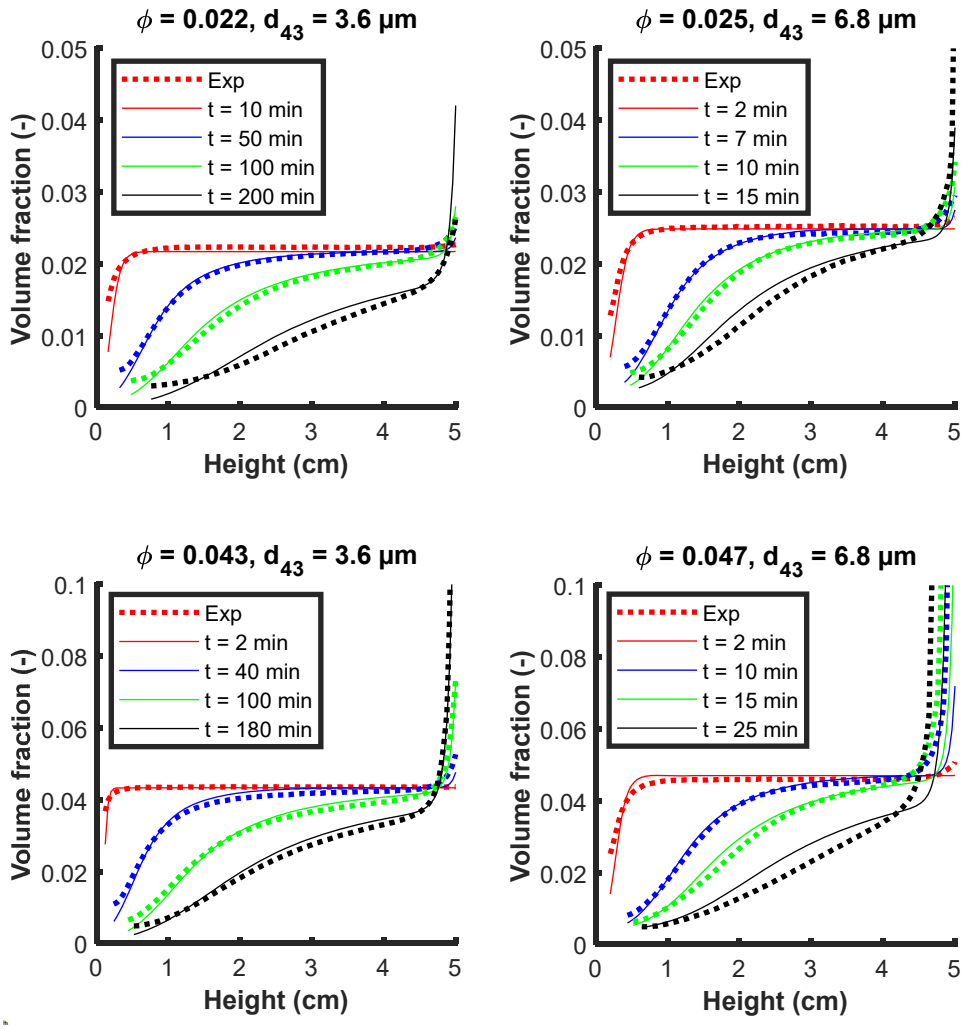

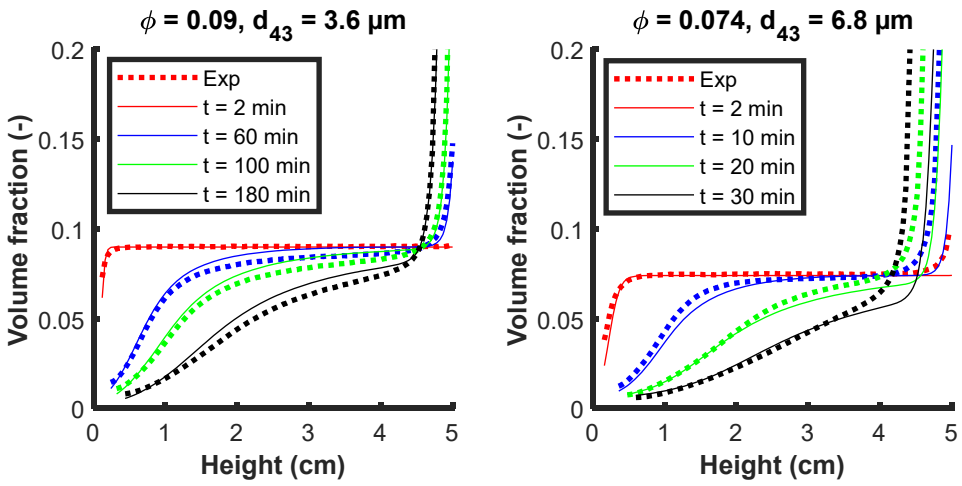

Figure 7: Fraction of oil as a function of the cell height, at selected times, for 6 experiments with different oil fractions and mean droplet diameter. The dotted lines refer to experimental data by turbidimetry and continuous lines are the model predictions.

In order to investigate the sensitivity of the model to the identified parameters, they were varied by simulation. Figure 8 shows the effect of the diffusion coefficient. It can be seen that the identified parameter $D = 1\times10^{-9}$ m² s^{-1} gives the optimal prediction of the experimental data. A lower D value leads to some oscillations in the creaming zone, while a higher value reduces the creaming rate.

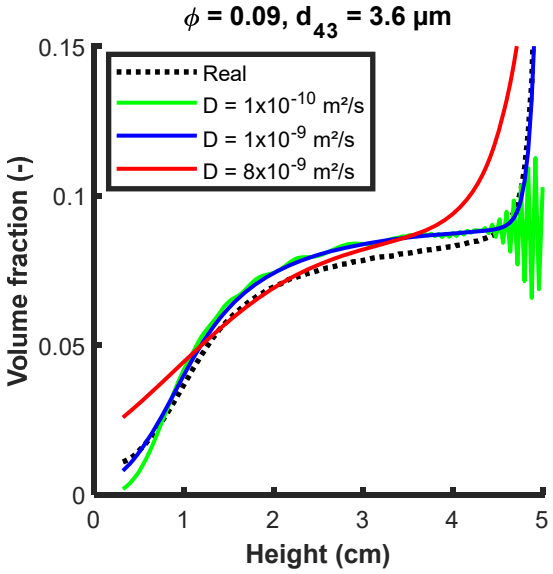

Figure 8: Fraction of oil as a function of the cell height after 100 min. The dotted lines refer to experimental data by turbidimetry and continuous lines are the model predictions with different D values.

The effect of the Richardson and Zaki parameter, n, is shown in Figure 9. A better fit to the experimental data is obtained with lower n values. However, with n =0, which means that we neglect the effect of the volume fraction on the creaming rate, the fit is not good at the top of the bottle, where the oil fraction increases importantly. Note that higher values, as suggested by Richardson and Zaki ($n = 4.65$) or Aleem and Mellon ($n = 2.3 - 5.5$)[4], slow down the creaming and do not fit the experimental data.

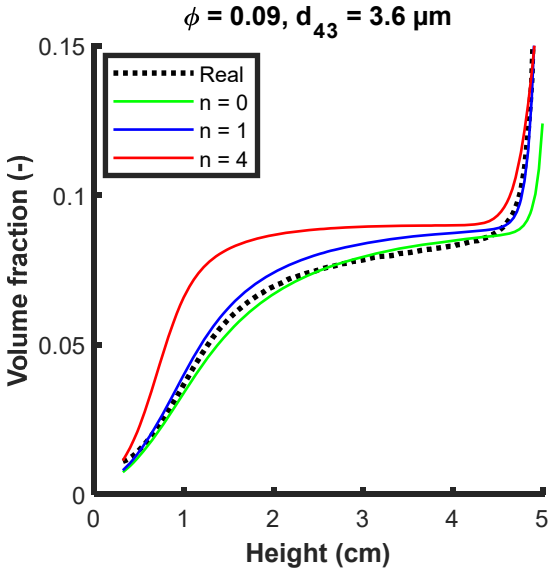

Figure 9: Fraction of oil as a function of the cell height after 100 min,. The dotted lines refer to experimental data by turbidimetry and continuous lines are the model predictions with different n values.

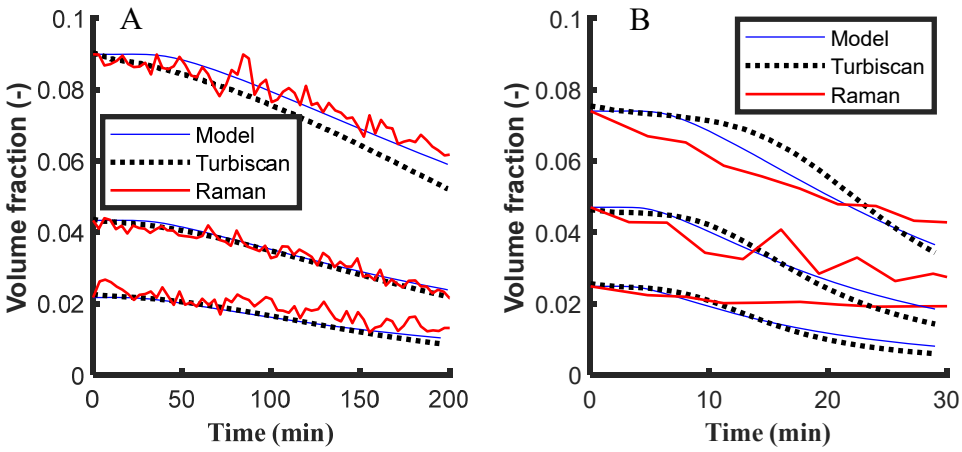

Figure 10: Concentration of oil at the middle height of the container as a function of time, as obtained by the Turbiscan, Raman spectroscopy and by the model. A: Experiments with $d_{43} = 3.6$ *µm at different initial oil fractions. B: Experiments with* $d_{43} = 6.8$ *µm.*

A comparison of the evolution of the volume fraction as a function of time, as obtained by the model, turbidimetry and Raman is shown in Figure 10A, for the sample with $d_{43} = 3.6$ µm at different initial oil fractions. The different measurements and the model predictions are comparable. However, larger differences are obtained for bigger droplets as shown in Figure 10B. The non-contact Raman mode was used for the sample with $d_{43} = 3.6$ µm for all volume fractions, and for the sample $d_{43} = 6.8$ µm at $\phi_T = 4.7$ %. The wet-head mode was employed in the samples $d_{43} = 6.8$ µm with $\phi_T = 2.56$ % and 7.4 %. Both Raman modes were found to have an equivalent performance. The prediction error may be due to the fact that the surface area of the peak does not necessarily evolve linearly with the concentration of oil or to a slight effect of the droplet size in the Raman spectra. A more advanced calibration of the Raman spectra could be helpful to eliminate the effect of the droplet size, and to be able to predict the concentration without the need to indicate the initial fraction. But, this would require a wider set of training data. Regarding the turbidimetry, it is much more sensitive to the droplet size than the Raman spectroscopy, and therefore a specific calibration was done for each emulsion.

However, as the emulsions contain droplets with a distribution of sizes that do not cream at the same velocity, a drift from the calibration model may occur with time.

Conclusions

The creaming behavior in O/W emulsions was investigated both experimentally and theoretically. At the experimental level, the use of a turbidimetry technique has the advantage of scanning the sample and giving backscattering at each height within time, which can be calibrated to predict the oil fraction. However, the prediction is very sensitive to the droplet size and a specific calibration is to be done for each range of sizes. Raman spectroscopy has the advantage of operating *in situ*, and the measurement is less sensitive to the droplet size, so it should be possible to have a single calibration for a wide range of droplet sizes. Also, the spectra demonstrated that the technology is sensitive to the creaming phenomenon. However, the presence of the probe may alter the creaming behavior and the droplets may get stuck on the probe.

A simple model was then developed and validated using turbidimetry experimental data under different operating conditions. A good prediction of the concentration of oil is obtained over height and time. The model could capture the effect of the droplet size on creaming, as bigger droplets appeared to be less stable. It also captured the effect of the oil fraction that hinders creaming when increased.

Acknowledgments

This work is funded by ModLife ITN. Grant agreement number 675251.

Highlights

- Creaming of emulsions is monitored using both turbidimetry and Raman spectroscopy

- The effect of droplet size distribution and oil volume fraction is investigated
- A mathematical model is developed to predict creaming of O/W emulsions

Nomenclature

A_d [$m^2.m^{-3}$]: surface area of droplets per unit volume of emulsion
a_s [$kg.m^{-3}$]: surface coverage of one molecule of surfactant
d_i [m]: representative diameter of droplets in the class i
d_{43} [m] : volume-based mean droplet diameter
D [$m^2.s^{-1}$]: diffusion coefficient
D_i [$m^2.s^{-1}$]: diffusion coefficient of droplets of diameter d_i
D_{i0} [$m^2.s^{-1}$]: Stokes-Einstein diffusivity of droplets of diameter d_i
g [$m.s^{-2}$]: gravity acceleration
m_s [$m^2.m^{-3}$]: surfactant concentration
$M_{w,s}$ [$kg.mol^{-1}$]: molecular weight of the surfactant
n [-]: Richardson-Zaki constant
N_a [-] : Avogadro number
S [m^2]: peak surface for Raman spectra
t [s]: time
u [$m.s^{-1}$]: hindered creaming velocity of the dispersed droplets
u_i [$m.s^{-1}$]: hindered creaming velocity of the dispersed droplets of size d_i
u_{ti} [$m.s^{-1}$]: terminal velocity of a single droplet of size d_i
z [m]: Spatial axis

Greek symbols

μ [Pa.s]: apparent dynamic viscosity of the fluid
μ_c [Pa.s]: dynamic viscosity of the continuous phase
μ_d [Pa.s]: dynamic viscosity of the dispersed phase
ρ_c [$kg.m^{-3}$]: density of the continuous phase
ρ_d [$kg.m^{-3}$]: density of the dispersed phase
ϕ [-]: dispersed phase volume fraction
ϕ_i [-]: volume fraction of the droplets of diameter d_i
ϕ_{max} [-]: maximum volume fraction of the dispersed phase
ϕ_T [-]: total dispersed phase volume fraction

Acknowledgement

This work was funded by ModLife ITN. Grant agreement number 675251.

References

(1) Tadros, T. F. Emulsion Formation, Stability, and Rheology. In *Emulsion Formation and Stability*; Tadros, T. F., Ed.; Wiley-VCH Verlag GmbH & Co. KGaA: Weinheim, Germany, 2013; pp 1–75.

(2) Borwankar, R. P.; Lobo, L. A.; Wasan, D. T. Emulsion Stability — Kinetics of Flocculation and Coalescence. *Colloids Surf.* **1992**, *69* (2–3), 135–146. https://doi.org/10.1016/0166-6622(92)80224-P.

(3) Trujillo-Cayado, L. A.; Santos, J.; Alfaro, M. C.; Calero, N.; Muñoz, J. A Further Step in the Development of Oil-in-Water Emulsions Formulated with a Mixture of Green Solvents. *Ind. Eng. Chem. Res.* **2016**, *55* (27), 7259–7266. https://doi.org/10.1021/acs.iecr.6b01320.

(4) Aleem, W.; Mellon, N.; Khan, J. A.; Al-Kayiem, H. H. Experimental Investigation and Mathematical Modeling of Oil/Water Emulsion Separation Effectiveness Containing Alkali-Surfactant-Polymer. *J. Dispers. Sci. Technol.* **2021**, *42* (9), 1286–1298. https://doi.org/10.1080/01932691.2020.1738244.

(5) Mcclements, D. J. Critical Review of Techniques and Methodologies for Characterization of Emulsion Stability. *Crit. Rev. Food Sci. Nutr.* **2007**, *47* (7), 611–649. https://doi.org/10.1080/10408390701289292.

(6) Chanamai, R.; McClements, D. J. Dependence of Creaming and Rheology of Monodisperse Oil-in-Water Emulsions on Droplet Size and Concentration. *Colloids Surf. Physicochem. Eng. Asp.* **2000**, *172* (1–3), 79–86. https://doi.org/10.1016/S0927-7757(00)00551-3.

(7) Chanamai, R.; McClements, D. J. Creaming Stability of Flocculated Monodisperse Oil-in-Water Emulsions. *J. Colloid Interface Sci.* **2000**, *225* (1), 214–218. https://doi.org/10.1006/jcis.2000.6766.

(8) Aleem, W.; Mellon, N. Model for the Prediction of Separation Profile of Oil-in-Water Emulsion. *J. Dispers. Sci. Technol.* **2018**, *39* (1), 8–17. https://doi.org/10.1080/01932691.2017.1288132.

(9) Abeynaike, A.; Sederman, A. J.; Khan, Y.; Johns, M. L.; Davidson, J. F.; Mackley, M. R. The Experimental Measurement and Modelling of Sedimentation and Creaming for Glycerol/Biodiesel Droplet Dispersions. *Chem. Eng. Sci.* **2012**, *79*, 125–137. https://doi.org/10.1016/j.ces.2012.05.036.

(10) Robins, M. M. Emulsions — Creaming Phenomena. *Curr. Opin. Colloid Interface Sci.* **2000**, *5* (5–6), 265–272. https://doi.org/10.1016/S1359-0294(00)00065-0.

(11) Lemarchand, C. Study of Emulsion Stabilization by Graft Copolymers Using the Optical Analyzer Turbiscan. *Int. J. Pharm.* **2003**, *254* (1), 77–82. https://doi.org/10.1016/S0378-5173(02)00687-7.

(12) Liu, J.; Huang, X.; Lu, L.; Li, M.; Xu, J.; Deng, H. Turbiscan Lab® Expert Analysis of the Biological Demulsification of a Water-in-Oil Emulsion by Two Biodemulsifiers. *J. Hazard. Mater.* **2011**, *190* (1–3), 214–221. https://doi.org/10.1016/j.jhazmat.2011.03.028.

(13) Jiang, T.; Hirasaki, G.; Miller, C.; Moran, K.; Fleury, M. Diluted Bitumen Water-in-Oil Emulsion Stability and Characterization by Nuclear Magnetic Resonance (NMR) Measurements. *Energy Fuels* **2007**, *21* (3), 1325–1336. https://doi.org/10.1021/ef0604487.

(14) Johns, M. L. NMR Studies of Emulsions. *Curr. Opin. Colloid Interface Sci.* **2009**, *14* (3), 178–183. https://doi.org/10.1016/j.cocis.2008.10.005.

(15) Simon, S.; Pierrard, X.; Sjöblom, J.; Sørland, G. H. Separation Profile of Model Water-in-Oil Emulsions Followed by Nuclear Magnetic Resonance (NMR) Measurements: Application Range and Comparison with a Multiple-Light Scattering Based Apparatus. *J. Colloid Interface Sci.* **2011**, *356* (1), 352–361. https://doi.org/10.1016/j.jcis.2011.01.012.

(16) Abeynaike, A.; Sederman, A. J.; Khan, Y.; Johns, M. L.; Davidson, J. F.; Mackley, M. R. The Experimental Measurement and Modelling of Sedimentation and Creaming for Glycerol/Biodiesel Droplet Dispersions. *Chem. Eng. Sci.* **2012**, *79*, 125–137.

(17) Fan, X.; Serale, G.; Capozzoli, A.; Perino, M. Experimental Measurement and Numerical Modeling of the Creaming of MPCM Slurry. *Energy Procedia* **2015**, *78*, 2010–2015. https://doi.org/10.1016/j.egypro.2015.11.192.

(18) Bury, M.; Gerhards, J.; Erni, W.; Stamm, A. Application of a New Method Based on Conductivity Measurements to Determine the Creaming Stability of o/w Emulsions. *Int. J. Pharm.* **1995**, *124* (2), 183–194. https://doi.org/10.1016/0378-5173(95)00075-T.

(19) Chanamai, R.; Herrmann, N.; McClements, D. J. Influence of Thermal Overlap Effects on the Ultrasonic Attenuation Spectra of Polydisperse Oil-in-Water Emulsions. *Langmuir* **1999**, *15* (10), 3418–3423. https://doi.org/10.1021/la981195f.

(20) Oshinowo, L. M.; Quintero, C. G.; Vilagines, R. D. CFD and Population Balance Modeling of Crude Oil Emulsions in Batch Gravity Separation—Comparison to Ultrasound Experiments. *J. Dispers. Sci. Technol.* **2016**, *37* (5), 665–675. https://doi.org/10.1080/01932691.2015.1054508.

(21) Patra, T.; Rinnan, Å.; Olsen, K. The Physical Stability of Plant-Based Drinks and the Analysis Methods Thereof. *Food Hydrocoll.* **2021**, *118*, 106770. https://doi.org/10.1016/j.foodhyd.2021.106770.

(22) Li, B.; Stenstrom, M. K. Research Advances and Challenges in One-Dimensional Modeling of Secondary Settling Tanks – A Critical Review. *Water Res.* **2014**, *65*, 40–63. https://doi.org/10.1016/j.watres.2014.07.007.

(23) Isfandiyar Kelbaliyev, G.; Babir Tagiyev, D.; Rizvan Manafov, M. Rheology of Structured Oil Emulsion. In *Nano- and Microencapsulation - Techniques and Applications*; Abu-Thabit, N., Ed.; IntechOpen, 2021. https://doi.org/10.5772/intechopen.92770.

(24) Stokes, G. G. *Mathematical and Physical Papers*; Cambridge University Press: Cambridge, 1850. https://doi.org/10.1017/CBO9780511702266.

(25) Robinson, C. D. Some Factors Influencing Sedimentation. *Ind. Eng. Chem.* **1926**, *18* (8), 869–871. https://doi.org/10.1021/ie50200a036.

(26) Richardson, J. F.; Zaki, W. N. The Sedimentation of a Suspension of Uniform Spheres under Conditions of Viscous Flow. *Chem. Eng. Sci.* **1954**, *3* (2), 65–73. https://doi.org/10.1016/0009-2509(54)85015-9.

(27) Kynch, G. J. A Theory of Sedimentation. *Trans. Faraday Soc.* **1952**, *48*, 166. https://doi.org/10.1039/tf9524800166.

(28) Davis, K. E.; Russel, W. B. An Asymptotic Description of Transient Settling and Ultrafiltration of Colloidal Dispersions. *Phys. Fluids Fluid Dyn.* **1989**, *1* (1), 82–100. https://doi.org/10.1063/1.857526.

(29) Wang, H.; Davis, R. H. Simultaneous Sedimentation and Coalescence of a Dilute Dispersion of Small Drops. *J. Fluid Mech.* **1995**, *295*, 247–261. https://doi.org/10.1017/S0022112095001959.

(30) Jeelani, S. A. K.; Hartland, S. Dynamic Response of Gravity Settlers to Changes in Dispersion Throughput. *AIChE J.* **1988**, *34* (2), 335–340.

(31) Jeelani, S. A. K.; Panoussopoulos, K.; Hartland, S. Effect of Turbulence on the Separation of Liquid−Liquid Dispersions in Batch Settlers of Different Geometries. *Ind. Eng. Chem. Res.* **1999**, *38* (2), 493–501. https://doi.org/10.1021/ie980436b.

(32) Yu, G.-Z.; Mao, Z.-S. Sedimentation and Coalescence Profiles in Liquid-Liquid Batch Settling Experiments. *Chem. Eng. Technol.* **2004**, *27* (4), 407–413. https://doi.org/10.1002/ceat.200401884.

(33) Aleem, W.; Mellon, N. Model for the Prediction of Separation Profile of Oil-in-Water Emulsion. *J. Dispers. Sci. Technol.* **2017**, 1–10. https://doi.org/10.1080/01932691.2017.1288132.

(34) Cunha, R. E. P.; Fortuny, M.; Dariva, C.; Santos, A. F. Mathematical Modeling of the Destabilization of Crude Oil Emulsions Using Population Balance Equation. *Ind. Eng. Chem. Res.* **2008**, *47* (18), 7094–7103. https://doi.org/10.1021/ie800391v.

(35) Grimes, B. A. Population Balance Model for Batch Gravity Separation of Crude Oil and Water Emulsions. Part I: Model Formulation. *J. Dispers. Sci. Technol.* **2012**, *33* (4), 578–590. https://doi.org/10.1080/01932691.2011.574946.

(36) Cai, X.; Chen, J.; Liu, M.; Ji, Y.; Ding, G.; Zhang, L. CFD Simulation of Oil–Water Separation Characteristics in a Compact Flotation Unit by Population Balance Modeling. *J. Dispers. Sci. Technol.* **2017**, *38* (10), 1435–1447. https://doi.org/10.1080/01932691.2016.1251323.

(37) Carnero Ruiz, C.; Molina-Bolívar, J.; Aguiar, J.; MacIsaac, G.; Moroze, S.; Palepu, R. Effect of Ethylene Glycol on the Thermodynamic and Micellar Properties of Tween 20. *Colloid Polym. Sci.* **2003**, *281* (6), 531–541. https://doi.org/10.1007/s00396-002-0801-1.

(38) Mengual, O. TURBISCAN MA 2000: Multiple Light Scattering Measurement for Concentrated Emulsion and Suspension Instability Analysis. *Talanta* **1999**, *50* (2), 445–456. https://doi.org/10.1016/S0039-9140(99)00129-0.

(39) Antonopoulou, E.; Rohmann-Shaw, C. F.; Sykes, T. C.; Cayre, O. J.; Hunter, T. N.; Jimack, P. K. Numerical and Experimental Analysis of the Sedimentation of Spherical Colloidal Suspensions under Centrifugal Force. *Phys. Fluids* **2018**, *30* (3), 030702. https://doi.org/10.1063/1.5010735.

(40) Taylor, G. I. The Viscosity of a Fluid Containing Small Drops of Another Fluid. *Proc. R. Soc. Math. Phys. Eng. Sci.* **1932**, *138* (834), 41–48. https://doi.org/10.1098/rspa.1932.0169.

(41) Corsetti, S.; Rabl, T.; McGloin, D.; Kiefer, J. Intermediate Phases during Solid to Liquid Transitions in Long-Chain n-Alkanes. *Phys. Chem. Chem. Phys.* **2017**, *19* (21), 13941–13950. https://doi.org/10.1039/C7CP01468F.

(42) Pal, R. Effect of Droplet Size on the Rheology of Emulsions. *AIChE J.* **1996**, *42* (11), 3181–3190. https://doi.org/10.1002/aic.690421119.